JASMAC
Conference of the Japan Society of Microgravity Application

OS2-6

静電浮遊炉を用いたレーザーアブレーション推力の計測および推力推定モデルの構築

Measurement of laser ablation thrust using an electrostatic levitation furnace and development of a thrust estimation model

國分ひなた [1], 森浩一 [1], 石川毅彦 [2], 小山千尋 [2], 織田裕久 [2],
Hinata KOKUBU[1], Koichi MORI[1], Takehiko ISHIKAWA[2], Chihiro KOYAMA[2] and Hirohisa ODA[2]
[1] 大阪公立大学大学院 工学研究科 航空宇宙海洋系専攻，Osaka Metropolitan University Aerospace Engineering,
[2]JAXA，Japan Aerospace Exploration Agency.

1. Introduction

In recent years, space debris have been increasing in number and has become an obstacle to space development. In particular, space debris of 1-10 cm in diameter cannot be observed from the ground and can totally destroy a spacecraft by collision. Therefore, debris removal by deorbit using laser ablation is promising. A scenario in which debris is deactivated and incinerated in the earth's atmosphere by irradiating it with a laser using a debris removal satellite has been proposed. In order to avoid debris splitting due to the use of high-power laser, the use of low-power and high-density laser is being considered. However, this removal method has not been realized. In order to achieve it, it is necessary to estimate the laser ablation thrust acting on the actual debris. Previous experiment measured laser ablation thrust in a thermally isolated environment using a ground-based electrostatic levitation reactor. However, this experiment had difficulties in levitating aluminum, the main material of debris, and convection currents in the metallic droplets caused the heat transfer coefficient to be different from that in the space environment. Therefore, in this study, we used the electrostatic levitation furnace (ELF) installed in the ISS to measure laser ablation thrust in the use of aluminum and in the space environment. In addition, a model for estimating the generated thrust from the viewpoint of heat conduction was constructed in a previous study, but it is not in sufficient agreement with the experimental results. Therefore, in this study, the heat conduction model was improved in parallel with the space experiment, and the mechanism of thrust generation was reexamined in order to complete a model that can quantitatively explain the results of the above-mentioned ground experiment.

2. Thrust Measurement Experiment

2.1. Experimental method

In this experiment, an ELF installed in the ISS was used. Figure 1 shows a schematic diagram of the ISS-ELF. The sample is floated stably in the chamber by adjusting the applied voltage to the top, bottom, left, and right electrodes by PD control based on a position sensor called IVS. The chamber is filled with Ar and the pressure is 2 atm. The experiment was divided into three stages: free drift experiments were conducted before, during, and after heating the sample. This experiment was filmed by a high-speed camera and a magnifying camera.

First, the metal sample is stably floated, and then the voltage applied to the sample is turned off to allow it to free-drift. When the sample moves 2mm from the initial position, the applied voltage is turned on again to return the sample to its initial position. This operation is hereinafter referred to as FD. Next, the sample is melted by four lasers mounted on the ELF. After confirming that the sample was floating stably after melting, the output of only one laser was reduced and FD was performed again. After that, all lasers were turned off, the sample was cooled, and FD was performed.

2.2. Analysis method

The forces acting on the sample are considered to be residual gravity, laser ablation thrust, and Coulomb force due to the voltage between the electrodes. In the following, the physical quantities before, during, and after heating are denoted by subscripts 1, 2, and 3. The control voltage is denoted by V, the offset voltage by V_r, the microgravity acceleration by G_μ, the electric charge in the sample by Q, and the distance between the electrodes by d.

The equation of motion of the sample at FD before heating is expressed by the following

$$m\ddot{\boldsymbol{x}}_{\boldsymbol{1}} = Q_1 \frac{\boldsymbol{V_r}}{\boldsymbol{d}} + m\boldsymbol{G_\mu}. \tag{1}$$

Next, the equation of motion of the sample in FD during heating is expressed by the following equation. Since the laser continues to irradiate the sample during heating FD, the thrust due to the laser is added to the

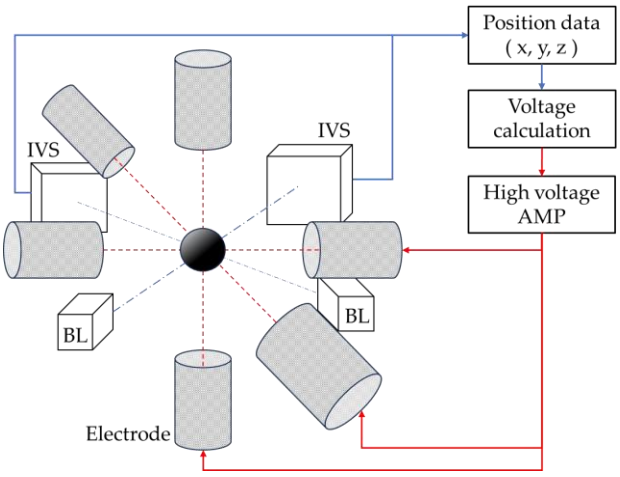

Figure 1. A schematic diagram of ISS-ELF

equation (1).

$$m\ddot{\boldsymbol{x}}_{\boldsymbol{2}} = Q_2 \frac{\boldsymbol{V}_r}{\boldsymbol{d}} + m\boldsymbol{G}_{\boldsymbol{\mu}} + \boldsymbol{F}_{laser}. \quad (2)$$

The equation of motion of a sample at FD after heating is expressed by the following

$$m\ddot{\boldsymbol{x}}_{\boldsymbol{3}} = Q_3 \frac{\boldsymbol{V}_r}{\boldsymbol{d}} + m\boldsymbol{G}_{\boldsymbol{\mu}}. \quad (3)$$

Here, the offset voltage is sufficiently small compared to the control voltage, and the microgravity is also sufficiently smaller than the Coulomb force due to the control voltage, so these forces can be considered negligible. Therefore, the equation of motion of a sample in stable suspension before heating can be transformed as follow:

$$m\ddot{\boldsymbol{x}}_{\boldsymbol{1}} = Q_1 \frac{\boldsymbol{V}}{\boldsymbol{d}}. \quad (4)$$

In the same way, the equation of motion of a sample in stable suspension after heating can be transformed as follow:

$$m\ddot{\boldsymbol{x}}_{\boldsymbol{3}} = Q_3 \frac{\boldsymbol{V}}{\boldsymbol{d}}. \quad (5)$$

Since the sample position is known from the IVS position detection data, the above equation can be used to calculate the charge on the sample before and after heating. With the charge known, the offset voltage and residual gravity can be calculated using equations (1) and (3). Finally, the laser ablation thrust is calculated using equation (2).

The energy conservation law of FD during heating is expressed as follow:

$$\frac{1}{2} m v_{fin}^2 = F_{laser} X + Q_2 \left(\frac{V_r X}{d}\right) + m G_\mu X, \quad (6)$$

where X is displacement and v_{fin} is velocity of the sample at the end of FD. The charge Q_2 and laser ablation thrust were obtained by solving equations (2) and (6) in series.

2.3. Experimental results

As an example of the experimental results, Figure 2 shows the IVS position detection and its fitting results. The IVS data were rounded to the first decimal place [1)], and the fitting was done as a quadratic function. After fitting in this way, the obtained function was used to calculate the generated thrust using the analytical method described in the previous section. The results of the thrust calculation are shown in Figure 3 and 4. Figure 3 shows that when the Al sample was irradiated with a laser power density of 4.6-5.6 [kW/cm^2], a thrust of 15 – 30 [nN] was generated. Figure 4 shows that when the Ti sample was irradiated with a laser power density of 18 to 20 [kW/cm^2], a thrust of 70 - 85 [nN] was generated. These results indicate that a thrust force is generated by the laser. It was also found that the laser power density was not dependent on the laser power density.

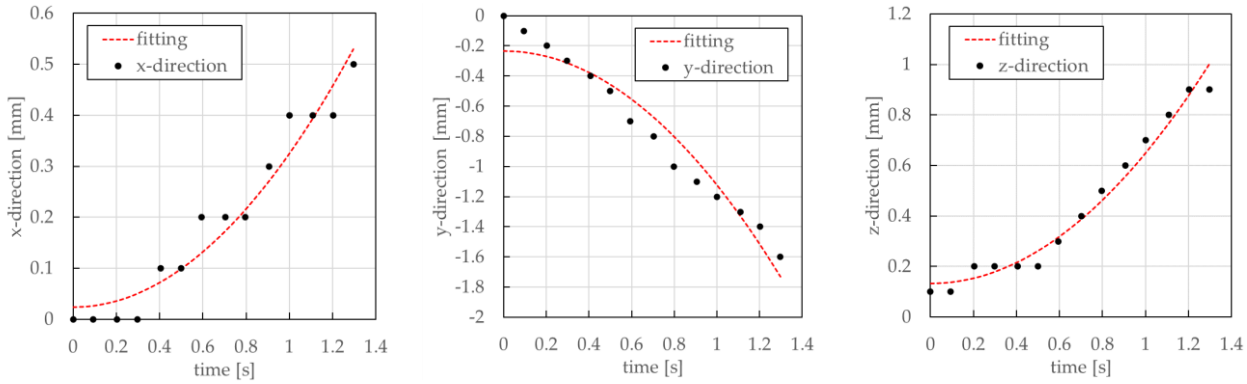

(a) x-direction (b) y-direction (c) z-direction

Figure 2. Example of position change in FD during heating

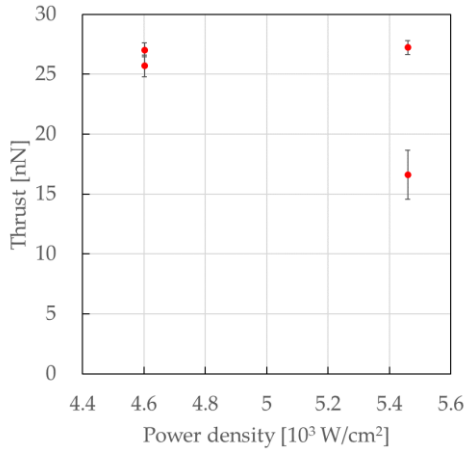

Figure 3. Laser thrust generated on the sample

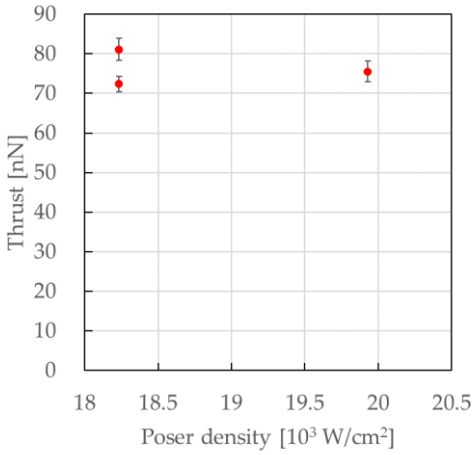

Figure 4. Laser thrust generated on the sample

3. Thrust Estimation Model

3.1. Thermal conductivity model

In this study, with the aim of completing a model that quantitatively explains the laser ablation thrust using a ground electrostatic levitation reactor, the thermal conduction model[3] constructed in the previous study was improved. The conceptual diagram is shown in Figure 5 and the procedure is as follows.

Ⅰ) The temperature increases locally due to heat input on the laser-irradiated surface.

Ⅱ) Inside the sample, heat is transferred based on a temperature gradient.

Ⅲ) The sample evaporates on the surface in response to temperature.

Ⅳ) Thrust is generated by the reaction of the impulse of the evaporated mass.

In step Ⅱ, the heat transfer is calculated by the following diffusion equation for heat conduction

$$\frac{\partial T}{\partial t} = \alpha \left(\frac{\partial^2 T}{\partial x^2} + \frac{\partial^2 T}{\partial y^2} + \frac{\partial^2 T}{\partial z^2} \right), \tag{7}$$

where T is temperature and α is thermal diffusivity. In addition, the following Neumann boundary conditions were defined from Fourier's law for the cells at the outer edges of the sample.

$$\lambda \frac{T_{i,j,k} - T_{i-1,j,k}}{\Delta t} = -\varepsilon\sigma \left(T_{i-1,j,k}^4 - T_\infty^4 \right) - JL, \tag{8}$$

where λ is thermal conductivity, ε is emissivity, σ is Stefan-Boltzmann constant, J is evaporation mass and L is latent heat. In step Ⅲ, the amount of evaporation is calculated by the Herz-Knudsen formula shown below.

$$J = \alpha P_W \sqrt{\frac{m}{2k_B T_W}}, \tag{9}$$

where P_W is surface pressure, m is molecular mass, k_B is Boltzmann constant and T_W is surface temperature. In step Ⅳ, the thermal velocity of the evaporating mass obtained in equation (9) was calculated from the temperature, and the impulse was obtained by multiplying it by the mass. The computational grid is considered to be a cubic lattice with 3-dimensional Cartesian coordinates. Furthermore, since the presence or absence of sample rotation during the experiment is unknown, constant velocity rotation around an axis perpendicular to the laser irradiation axis was considered as a simplified rotation model.

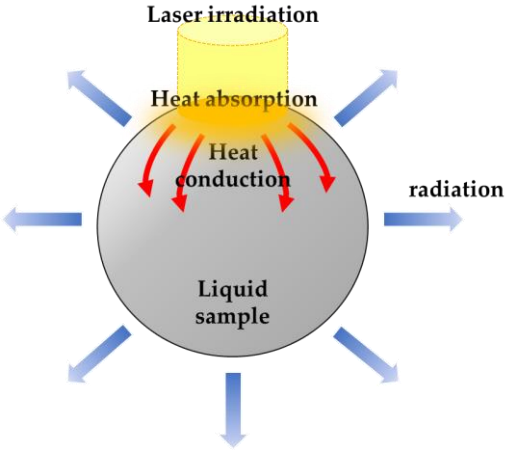

Figure 5. Conceptual diagram of heat transfer model

3.2. Simulation results and Future vision

The results of numerical simulation under the experimental conditions shown in the Table 1 are shown in the figure 6. Here, T_m is the temperature at boiling point. The emissivity and absorptivity were experimentally determined to be close to the experimental and simulated results, since they were unknown for the liquid metal. Overlapping of the graphs was based on laser power output. The figure 6 shows that sufficient agreement was obtained for the temperature. However, the thrust was about 100 times larger than the experimental value, as shown in the figure 6. Furthermore, while a part of the experimental thrust appears to be in a steady state, the simulation results show no such behavior. These results indicate that while the heat transfer model for estimating temperature can be considered complete, the model for calculating thrust is not adequate. Therefore, the method of generating thrust is currently being reexamined from the viewpoint of external gas analysis, leaving the heat conduction model intact.

Table 1. Simulation conditions

Sample	Zr
Specific heat	436 J/(kg・K)
Emissivity	0.13
Absorption rate	0.17
Density	$6782-0.27T$ kg/m^3
Thermal conductivity	$94.61+0.0441(T-T_m)$ W/(m・K)
Vapor pressure	$10^{11.812-30295/T}$ Pa

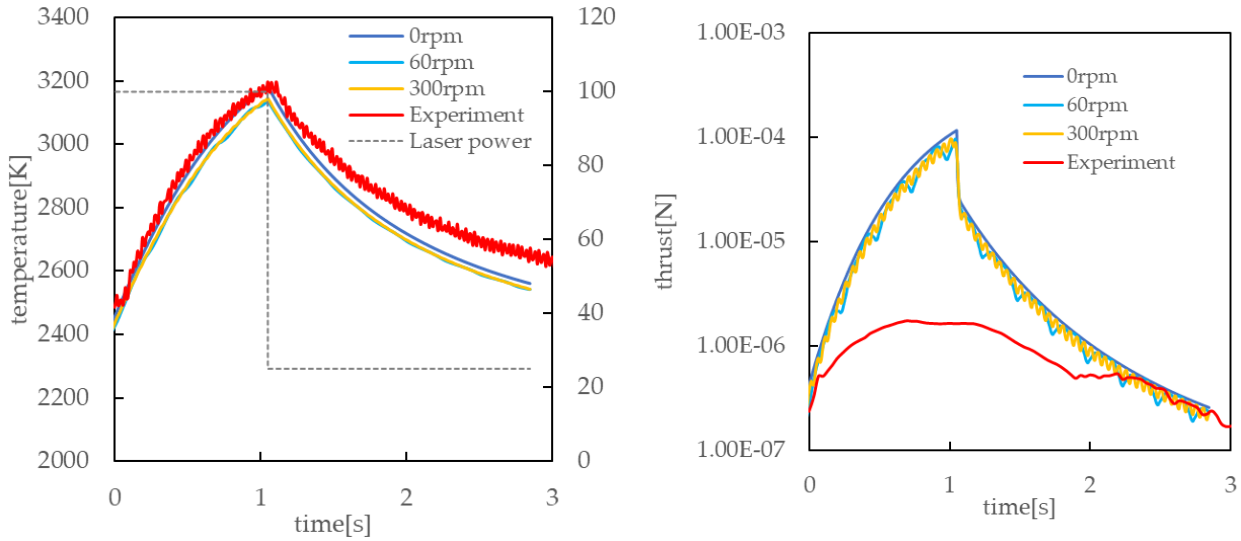

(a) Comparison of temperature (b) Comparison of thrust

Figure 6. Comparison of experimental and simulation results

Acknowledgement

I would like to thank the researchers at JAXA's Ishikawa Laboratory for allowing us to use their electrostatic levitation furnace as an experimental device, for their advice and cooperation on experimental methods, and for giving us the opportunity to conduct on-orbit experiments on the ISS. I would like to take this opportunity to express our deepest gratitude.

References

1) Takehiko ISHIKAWA, Chihiro KOYAMA, Haruka TAMARU, Hideki SARUWATARI, Masato OHSHIO and Yasuhiro NAKAMURA, Status of the Electrostatic Levitation Furnace in the ISS –Evaluation of Sample Position Control-, International Journal of Microgravity Science and Application, 2018, Volume 35, 2, 35025.
2) Naoki, MINAGAWA, Measurement of thrust generated by low-power CW laser irradiation of metallic droplets in an electrostatic levitation furnace, master's thesis for Osaka Metropolitan University, 2023.
3) Tomoya AKITA, Experiments on thrust measurement by CW laser ablation using an electrostatic levitation furnace and development of a thrust generation model, master's thesis for Nagoya University, 2022.
4) Yuri B. Zudin, Non-equilibrium Evaporation and Condensation Processes, 3rd Ed, pp.17-24.
5) Paul-Francois Paradis and Won-Kyu Rhim. Thermophysical properties of zirconium at high temperature. *Journal of Materials Research*, Vol. 14, No.9, pp.3713-3719, 1999.
6) Aaron J. Rulison and Won-Kyu Rhim. Constantpressure specific heat to hemispherical total emissivity ratio for undercooled liquid nickel, Zirconium, and Silicon. *Metalluragical and Materials Transactions B*, Vol. 26, 1995.
7) Bonnell, D. W. , Treverton, J. A. , Valerga, A. J. , Margrave, J. L. The emissivities of liquid metals at their fusion temperature. 1972.